Two-dimensional quantum dots in high magnetic fields:
Rotating-electron-molecule versus composite-fermion approach

Constantine Yannouleas* and Uzi Landman[†]

School of Physics, Georgia Institute of Technology, Atlanta, Georgia 30332-0430, USA
(Received 24 February 2003; revised manuscript received 30 April 2003; published 28 July 2003)

Exact diagonalization results are reported for the lowest rotational band of $N=6$ electrons in strong magnetic fields in the range of high angular momenta, $70 \leq L \leq 140$ (covering the corresponding range of fractional filling factors, $1/5 \geq \nu \geq 1/9$). A detailed comparison of energetic, spectral, and transport properties (specifically, magic angular momenta, radial electron densities, occupation number distributions, overlaps and total energies, and exponents of current-voltage power law) shows that the recently discovered rotating-electron-molecule wave functions [Phys. Rev. B **66**, 115315 (2002)] provide a superior description compared to the composite-fermion–Jastrow-Laughlin ones.

I. INTRODUCTION

Two-dimensional (2D) N-electron systems (with a small finite N) in strong magnetic fields (B) have been the focus of extensive theoretical investigations in the last 20 years.[1–17] The principal motivations for these research activities are (I) the early realization[1,2] that certain special states of few-electron systems are relevant[18] through appropriate analogies to the physics of the fractional quantum Hall effect (FQHE), observed in the infinite 2D electron gas; (II) the unavoidable necessity, due to computer limitations, to test proposed model wave functions for the FQHE through numerical calculations for finite-size systems; and (III) the recent progress in nanofabrication techniques at semiconductor interfaces that has allowed experiments on 2D quantum dots (QD's), with refined control of their size, shape, and number of electrons[19–21] (down to a few electrons).

The physics of such systems (i.e., QD's in high B) is most often described with the use of composite-fermion[4]–Jastrow-Laughlin[1] (CF-JL) analytic trial wave functions in the complex plane. However, it is well known that the thematic framework of the CF-JL approach is built on the so-called Jastrow correlations associated with a particular short-range interparticle repulsion.[22] In a recent paper,[15] using as a thematic basis the picture of collectively rotating electron (or Wigner) molecules (REM's), we have derived a different class of analytic and parameter-free trial wave functions. The promising property of these REM wave functions is that, unlike the CF-JL ones, they capture the all-important correlations arising from the long-range character of the Coulomb force.

In this paper, we present an in-depth assessment of the CF-JL and REM trial wave functions regarding their ability to approximate the exact wave functions in the case of QD's (this case is often referred to as the "disk geometry" in the FQHE literature). First systematic exact diagonalization (EXD) results are reported here for the lowest rotational band of $N=6$ electrons in strong magnetic fields in the range of high angular momenta $70 \leq L \leq 140$ (covering the corresponding range of fractional filling factors,[23] $1/5 \geq \nu \geq 1/9$). A detailed comparison (addressing five properties: i.e., the

prediction of magic angular momenta, radial electron densities, occupation number distributions, overlaps and total energies, and exponents of current-voltage power law) shows that the REM wave functions yield a superior description to that obtained through the composite-fermion–Jastrow-Laughlin ones.

The plan of this paper is as follows: Section II presents an outline of the REM theory, while Sec. III focuses on a brief review of the composite-fermion approach. Exact diagonalization results and comparisons with the CF-JL and REM wave functions are presented in Sec. IV. Finally, our results are summarized in Sec. V.

II. OUTLINE OF REM THEORY

In the last eight years and, in particular, since 1999 [when it was demonstrated[24] that Wigner crystallization is related to symmetry breaking at the *unrestricted* Hartree-Fock (UHF) mean-field level], the number of publications[8–17,24–40] addressing the formation and properties of Wigner (or electron) molecules in 2D QD's and quantum dot molecules has grown steadily. A consensus has been reached that rotating electron molecules are formed both in zero[12,24–40] and high[8–17] magnetic fields.

At $B=0$, the formation of REM's in QD's is analogous to Wigner crystallization in infinite 2D media; i.e., when the strength of the interelectron repulsion relative to the zero-point kinetic energy (R_W) exceeds a certain critical value, electrons spontaneously crystallize around particular sites, forming geometric molecular structures. At high magnetic fields, the formation of Wigner molecules may be thought of as involving a two-step crystallization process: (I) the localization of electrons results from the shrinkage of the orbitals due to the increasing strength of the magnetic field and (II) then even a weak interelectron Coulomb repulsion is able to arrange the localized electrons according to geometric molecular structures (thus this process is independent of the value of R_W). It has been found[8,10,12] that the molecular structures at high B coincide with the equilibrium configurations at $B=0$ of N classical point charges.[41,42]

Due to the finite number N of electrons, however, there are two crucial differences between the REM and bulk

Wigner crystal. Namely, (I) the crystalline structure is that of the equilibrium 2D configuration of N classical point charges and, thus, consists of nested polygonal rings[43] and (II) the Wigner molecules rotate as a whole (collective rotations) in analogy with the case of 3D natural molecules.

A most striking observation concerning the REM's is that their formation and properties have been established with the help of traditional *ab initio* many-body methods: i.e., exact diagonalization,[9–11,16,25,27,38] quantum Monte Carlo[26,29,33,39] (QMC), and the systematic controlled hierarchy[8,12,15,17,24,34,35,40] of approximations involving the UHF and subsequent post-Hartree-Fock methods. This contrasts with the case of the CF-JL wave functions, which were inspired through "intuition-based guesswork."

In spite of its firm foundation in many-body theory, however, the REM picture has not, until recently, successfully competed with the CF-JL picture; indeed many research papers[44–51] and books[18] describe the physics of QD's in high magnetic fields following exclusively notions based on CF-JL functions, as expounded in 1983 (see Ref. 1) and developed in detail in 1995 in Ref. 6 and Ref. 7. We believe that one of the main obstacles for more frequent use of the REM picture has been the lack of analytic correlated wave functions associated with this picture. This situation, however, has changed with the recent explicit derivation of such REM wave functions.[15]

The approach used in Ref. 15 for constructing the REM functions in high B consists of two steps: First the breaking of the rotational symmetry at the level of the single-determinantal unrestricted Hartree-Fock approximation yields states representing electron molecules (or finite crystallites, also referred to as Wigner molecules; see Ref. 24 and Ref. 12). Subsequently the rotation of the electron molecule is described through restoration of the circular symmetry via post Hartree-Fock methods and, in particular, projection techniques.[52] Naturally, the restoration of symmetry goes beyond the single-determinantal mean-field description and yields multideterminantal wave functions. For QD's, we have shown that the method of symmetry restoration is applicable to both the zero-[34,40] and high-[15] magnetic-field cases.

In the zero- and low-field cases, the broken-symmetry UHF orbitals need to be determined numerically, and, in addition, the restoration of the total-spin symmetry needs to be considered for unpolarized and partially polarized cases. The formalism and mathematical details of this procedure at $B = 0$ have been elaborated in Ref. 34 (see also Ref. 53 and Ref. 54) for the restoration of the total spin in the case of quantum dot molecules).

In the case of high magnetic fields, one can specifically consider the limit when the confining potential can be neglected compared to the confinement induced by the magnetic field. Then, assuming a symmetric gauge, the UHF orbitals can be represented[15,55] by displaced Gaussian analytic functions, centered at different positions $Z_j \equiv X_j + \iota Y_j$ according to the equilibrium configuration of N classical point charges[41,42] arranged at the vertices of nested regular polygons (each Gaussian representing a localized electron). Such

displaced Gaussians are written as (here and in the following $\iota \equiv \sqrt{-1}$)

$$u(z,Z_j) = (1/\sqrt{\pi}) \exp[-|z-Z_j|^2/2] \exp[-\iota(xY_j - yX_j)], \tag{1}$$

where the phase factor is due to the gauge invariance. $z \equiv x + \iota y$ (see Ref. 56), and all lengths are in dimensionless units of $l_B\sqrt{2}$ with the magnetic length being $l_B = \sqrt{\hbar c/eB}$.

In Ref. 15, we used these analytic orbitals to first construct the broken-symmetry UHF determinant Ψ_N^{UHF} and then proceeded to derive analytic expressions for the many-body REM wave functions by applying onto Ψ_N^{UHF} an appropriate projection operator[15] $\mathcal{O}_L$ that restores the circular symmetry and generates *correlated*[57] wave functions with good total angular momentum L. These REM wave functions can be easily written down[15] in second-quantized form for any classical polygonal ring arrangement $(n_1, n_2, \dots)$ by following certain simple rules for determining the coefficients of the determinants, $D(l_1, l_2, \dots, l_N) \equiv \det[z_1^{l_1}, z_2^{l_2}, \dots, z_N^{l_N}]$, where the l_j's denote the angular momenta of the individual electrons. Since we will focus here on the case of $N = 6$ and $N = 3$ electrons, we list for completeness the REM functions associated with the $(0,N)$ and $(1,N-1)$ ring arrangements, respectively [here $(0,N)$ denotes a regular polygon with N vertices, such as an equilateral triangle or a regular hexagon, and $(1,N-1)$ is a regular polygon with $N-1$ vertices and one occupied site in its center],

$$\Phi_L(0,N) = \sum_{\substack{l_1+\cdots+l_N=L \\ 0 \leq l_1 < l_2 < \cdots < l_N}} \left(\prod_{i=1}^{N} l_i!\right)^{-1}$$
$$\times \left(\prod_{1 \leq i < j \leq N} \sin\left[\frac{\pi}{N}(l_i - l_j)\right]\right)$$
$$\times D(l_1, l_2, \dots, l_N) \exp\left(-\sum_{i=1}^{N} z_i z_i^*/2\right), \tag{2}$$

with

$$L = L_0 + Nm, \quad m = 0,1,2,3,\dots, \tag{3}$$

and

$$\Phi_L(1,N-1) = \sum_{\substack{l_2+\cdots+l_N=L \\ 1 \leq l_2 < l_3 < \cdots < l_N}} \left(\prod_{i=2}^{N} l_i!\right)^{-1}$$
$$\times \left(\prod_{2 \leq i < j \leq N} \sin\left[\frac{\pi}{N-1}(l_i - l_j)\right]\right)$$
$$\times D(0,l_2, \dots, l_N) \exp\left(-\sum_{i=1}^{N} z_i z_i^*/2\right), \tag{4}$$

with

$$L = L_0 + (N-1)m, \quad m = 0,1,2,3,\dots, \tag{5}$$

where $L_0 = N(N-1)/2$ is the minimum allowed total angular momentum for N (polarized) electrons in high magnetic fields.

Notice that the REM wave functions [Eq. (2) and Eq. (4)] vanish identically for values of the total angular momenta outside the specific values given by Eq. (3) and Eq. (5), respectively.

III. OUTLINE OF COMPOSITE-FERMION THEORY

According to the CF picture,[6] the many-body wave functions in high magnetic fields that describe N electrons in the disk geometry (case of 2D QD's) are given by the expression

$$\Phi_L^{CF}(N) = \mathcal{P}_{LLL} \prod_{1 \leq i < j \leq N} (z_i - z_j)^{2m} \Psi_{L*}^{IPM}, \quad (6)$$

where $z = x + \iota y$ and Ψ_{L*}^{IPM} is the Slater determinant of N *noninteracting* electrons of total angular momentum $L*$; it is constructed according to the independent particle model (IPM) from the Darwin-Fock[58] orbitals $\psi_{p,l}(z)$, where p and l are the number of nodes and the angular momentum, respectively [for the values of p and l in the nth Landau level in high B, see the paragraph following Eq. (7) below].

The Jastrow factor in front of Ψ_{L*}^{IPM} is introduced to represent the effect of the interelectron Coulombic interaction. In the CF literature, this assumption is often described by saying that "the Jastrow factor binds $2m$ vortices to each electron of Ψ_{L*}^{IPM} to convert it into a composite fermion."

The single-particle electronic orbitals in the Slater determinant Ψ_{L*}^{IPM} are not restricted to the lowest Landau level (LLL). As a result, it is necessary to apply a projection operator $\mathcal{P}_{LLL}$ to guarantee that the CF wave function lies in the LLL, as appropriate for $B \to \infty$.

Since the CF wave function is an homogeneous polynomial in the electronic positions z_j's, its angular momentum L is related to the noninteracting total angular momentum $L*$ as follows:

$$L = L* + mN(N-1) = L* + 2mL_0. \quad (7)$$

There is no reason to *a priori* restrict the Slater determinants Ψ_{L*}^{IPM} to a certain form, but according to Ref. 6, such a restriction is absolutely necessary in order to derive systematic results. Thus following Ref. 6, henceforth, we will restrict the noninteracting $L*$ to the range $-L_0 \leq L* \leq L_0$, and we will assume that the Slater determinants Ψ_{L*}^{IPM} are the so-called compact ones. Let N_n denote the number of electrons in the nth Landau level (LL) with $\Sigma_{n=0}^t N_n = N$; t is the index of the highest occupied LL and all the lower LL's with $n \leq t$ are assumed to be occupied. The compact determinants are defined as those in which the N_n electrons occupy contiguously the single-particle orbitals (of each nth LL) with the lowest angular momenta, $l = -n, -n+1, \ldots, -n+N_n - 1$ $[p + (|l| - l)/2 = n]$. The compact Slater determinants are usually denoted as $[N_0, N_1, \ldots, N_t]$, and the corresponding total angular momenta are given by $L* = (1/2)\Sigma_{s=0}^t N_s(N_s - 2s - 1)$.

Most important for our present study is the fact that the Jastrow-Laughlin wave functions with angular momentum $L = (2m+1)L_0$ [corresponding to fractional filling factors $\nu = L_0/L = 1/(2m+1)$],

$$\Phi_L^{JL}(N) = \prod_{1 \leq i < j \leq N} (z_i - z_j)^{2m+1} \exp\left(-\sum_{k=1}^N z_k z_k^*/2 \right), \quad (8)$$

are a special case of the CF functions for $L* = L_0$, i.e.,

$$\Phi_L^{JL}(N) = \Phi_L^{CF}(N; L* = L_0), \quad L = (2m+1)L_0. \quad (9)$$

Note that for $L* = L_0$, all the noninteracting electrons occupy contiguous states in the LLL ($n = 0$) with $l = 0, 1, \ldots, N-1$.

The CF-JL wave functions [Eqs. (6) and (8)] are represented by compact, one-line mathematical expressions, which, however, are not the most convenient for carrying out numerical calculations. Numerical studies of the CF-JL functions usually employ sophisticated Monte Carlo computational techniques. The REM wave functions, on the other hand, are by construction expressed in second-quantized (superposition of Slater determinants) form, precisely like the wave functions from exact diagonalization, a fact that greatly simplifies the numerical work. In the numerical calculations involving JL wave functions in this paper, we have circumvented the need to use Monte Carlo techniques, since we were able to determine the Slater decomposition[59] of the JL states with the help of the symbolic language MATHEMATICA.[60]

We stress again that, unlike the REM functions, the CF-JL wave functions have not been derived microscopically—i.e., from the many-body Schrödinger equation with interelectron Coulombic repulsions. Attempts have been made to justify them *a posteriori* by pointing out that their overlaps with exact wave functions are close to unity or that their energies are close to the exact energies. However, we will show below that this agreement is limited to rather narrow ranges of filling factors at $1 \geq \nu \geq 1/3$ or to small electron numbers N; as soon as one extends the comparisons to a broader range of ν's for $N \geq 6$, as well as to other quantities like electron densities and occupation number distributions, this agreement markedly deteriorates.

IV. EXACT DIAGONALIZATION RESULTS AND COMPARISONS

In the case of high magnetic fields, the Hilbert space for exact diagonalization calculations can be restricted to the LLL and many such calculations have been reported[2,3,5,9,10,18,44,46,61–64] in the past 20 years. However, for $N \geq 5$, such EXD studies have been restricted to angular momenta corresponding to a rather narrow range of fillings factors, $1 \geq \nu \geq 1/3$.

In this paper, we have performed systematic EXD calculations in the LLL for $N = 6$ electrons covering the much broader range of fillings factors $1 \geq \nu \geq 1/9$; such a range corresponds to angular momenta $15 \leq L \leq 140$ (note that for $\nu = 1/3$ one has $L = 45$). Of crucial importance for extending
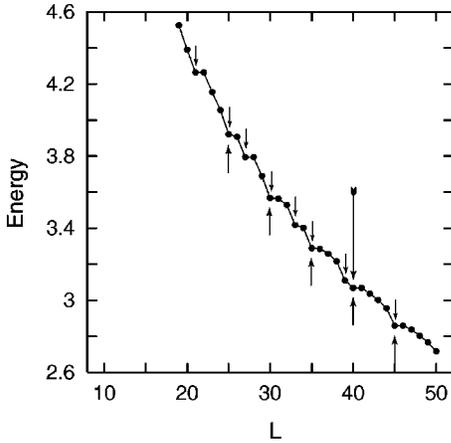
FIG. 1. Total interaction energy from exact diagonalization calculations as a function of the total angular momentum ($10 \leq L \leq 50$) for $N=6$ electrons in high magnetic field. The upwards pointing arrows indicate the magic angular momenta corresponding to the classically most stable (1,5) polygonal ring arrangement of the Wigner molecule. The short downwards pointing arrows indicate successful predictions of the composite-fermion model. The long downward arrow indicates a magic angular momentum not predicted by the CF model. Energies in units $e^2/\kappa l_B$, where κ is the dielectric constant.

the calculations to such large L's has been our use of Tsiper's[65] analytic formula for calculating the two-body matrix elements of the Coulomb interelectron repulsion; this formula expresses the matrix elements as finite sums of positive terms. Earlier analytic formulas[3] suffered from large cancellation errors due to summations over alternating positive and negative terms. At the same time, Tsiper's formula is computationally faster compared to the slowly convergent series of Ref. 61.

For the solution of the large scale, but sparse, Coulomb eigenvalue problem, we have used the ARPACK computer code.[66] For a given L, the Hilbert space is built out of Slater determinants,

$$D(l_1,l_2,\ldots,l_N)\exp\left(-\sum_{i=1}^{N} z_i z_i^*/2\right), \qquad (10)$$

with

$$l_1 < l_2 < \cdots < l_N, \qquad \sum_{k=1}^{N} l_k = L, \qquad (11)$$

and its dimensions are controlled by the maximum allowed single-particle angular momentum l_{max}, such that $l_k \leq l_{max}$, $1 \leq k \leq N$. We have used $l_{max} = l_{max}^{JL} + 5 = 10(m+1)$ (see Ref. 59 for the definition of l_{max}^{JL}) for each group of angular momenta L corresponding to the range $1/(2m+1) \leq \nu < 1/(2m-1)$, $m=1,2,3,4$. For example, for $L=105$, $l_{max}=40$ and the dimension of the Hilbert space is 56 115; for $L=135$, $l_{max}=50$ and the size of the Hilbert space is 187 597. By varying l_{max}, we have checked that this choice produces well converged numerical results.
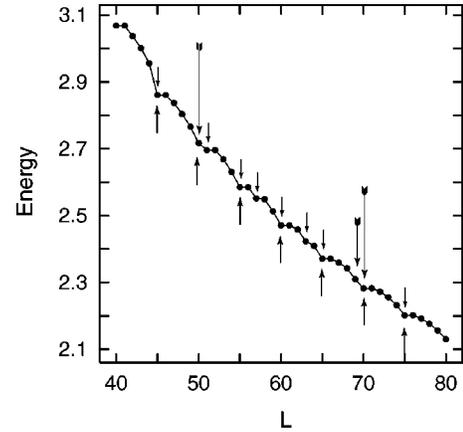
FIG. 2. Total interaction energy from exact diagonalization calculations as a function of the total angular momentum ($40 \leq L \leq 80$) for $N=6$ electrons in high magnetic field. The upwards pointing arrows indicate the magic angular momenta corresponding to the classically most stable (1,5) polygonal ring arrangement of the Wigner molecule. The short downwards pointing arrows indicate successful predictions of the composite-fermion model. The medium-size downwards pointing arrow indicates a prediction of the CF model that fails to materialize as a magic angular momentum. The long downward arrows indicate magic angular momenta not predicted by the CF model. Energies in units of $e^2/\kappa l_B$, where κ is the dielectric constant.

A. Predictions of magic angular momenta

For $N=6$, Figs. 1–4 display (in four installments) the total interaction energy from EXD as a function of the total angular momentum L in the range $19 \leq L \leq 140$. (The total
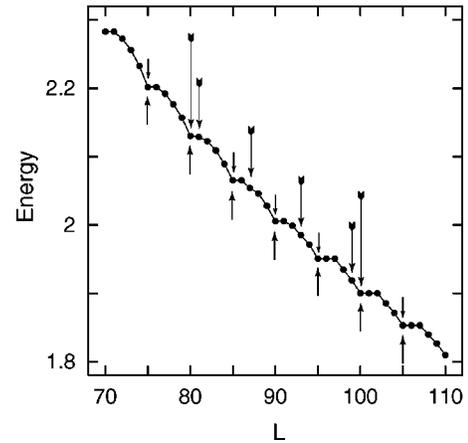
FIG. 3. Total interaction energy from exact diagonalization calculations as a function of the total angular momentum ($70 \leq L \leq 110$) for $N=6$ electrons in high magnetic field. The upwards pointing arrows indicate the magic angular momenta corresponding to the classically most stable (1,5) polygonal ring arrangement of the Wigner molecule. The short downwards pointing arrows indicate successful predictions of the composite-fermion model. The medium-size downwards pointing arrows indicate predictions of the CF model that fail to materialize as magic angular momenta. The long downward arrows indicate magic angular momenta not predicted by the CF model. Energies in units of $e^2/\kappa l_B$, where κ is the dielectric constant.
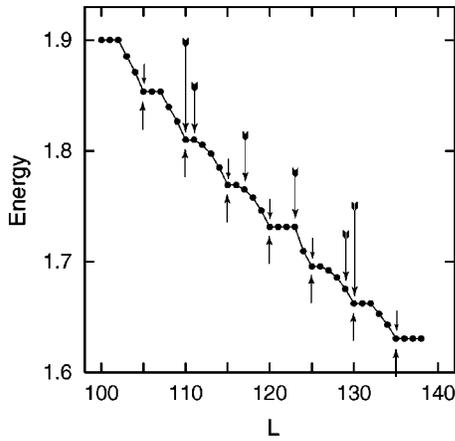
FIG. 4. Total interaction energy from exact diagonalization calculations as a function of the total angular momentum ($100 \leq L \leq 140$) for $N = 6$ electrons in high magnetic field. The upwards pointing arrows indicate the magic angular momenta corresponding to the classically most stable (1,5) polygonal ring arrangement of the Wigner molecule. The short downwards pointing arrows indicate successful predictions of the composite-fermion model. The medium-size downwards pointing arrows indicate predictions of the CF model that fail to materialize as magic angular momenta. The long downward arrows indicate magic angular momenta not predicted by the CF model. Energies in units of $e^2/\kappa l_B$, where κ is the dielectric constant.

TABLE I. Compact noninteracting Slater determinants and associated angular momenta L^* for $N = 6$ electrons according to the CF presciption. Both $L^* = -3$ and $L^* = 3$ are associated with two compact states each, the one with lowest energy being the preferred one.

Compact state	L^*
[1,1,1,1,1,1]	−15
[2,1,1,1,1]	−9
[2,2,1,1]	−5
[3,1,1,1]	−3
[2,2,2]	−3
[3,2,1]	0
[4,1,1]	3
[3,3]	3
[4,2]	5
[5,1]	9
[6]	15

kinetic energy, being a constant, can be disregarded.) One can immediately observe the appearance of downward cusps, implying states of enhanced stability, at certain "magic angular momenta."

For the CF theory, the magic angular momenta can be determined by Eq. (7), if one knows the noninteracting L^*'s; the CF magic L's in any interval $1/(2m-1) \geq \nu \geq 1/(2m+1)$ [$15(2m-1) \leq L \leq 15(2m+1)$], $m = 1,2,3,4,\dots$, can be found by adding $2mL_0 = 30m$ units of angular momentum to each of the L^*'s. To obtain the noninteracting L^*'s, one needs first to construct[6,9] the compact Slater determinants. The compact determinants and the corresponding noninteracting L^*'s are listed in Table I.

There are nine different values of L^*'s, and thus the CF theory for $N = 6$ predicts that there are always nine magic numbers in any interval $15(2m-1) \leq L \leq 15(2m+1)$ between two consecutive JL angular momenta $15(2m-1)$ and $15(2m+1)$, $m = 1,2,3,\dots$ (henceforth we will denote this interval as $\mathcal{I}_m$). For example, using Table I and Eq. (7), the CF magic numbers in the interval $15 \leq L \leq 45$ ($m = 1$) are found to be the following nine:[67]

$$15, \ 21, \ 25, \ 27, \ 30, \ 33, \ 35, \ 39, \ 45. \qquad (12)$$

On the other hand, in the interval $105 \leq L \leq 135$ ($m = 4$), the CF theory predicts the following set of nine magic numbers,

$$105, \ 111, \ 115, \ 117, \ 120, \ 123, \ 125, \ 129, \ 135. \qquad (13)$$

An inspection of the total-energy–vs–L plots in Figs. 1–4 reveals that the CF prediction badly misses the actual magic angular momenta specified by the EXD calculations as those associated with the downward cusps. Indeed it is immediately apparent that the number of downward cusps in any interval $\mathcal{I}_m$ is always different from 9. Indeed, there are 10 cusps in $\mathcal{I}_1$ (including that at $L = 15$, not shown in Fig. 1), 10 in $\mathcal{I}_2$ (see Fig. 2), 7 in $\mathcal{I}_3$ (see Fig. 3), and 7 in $\mathcal{I}_4$ (see Fig. 4). In detail, the CF theory fails in the following two aspects: (I) There are exact magic numbers that are consistently missing from the CF prediction in every interval; with the exception of the lowest $L = 20$, these *exact* magic numbers (marked by a long downward arrow in the figures) are given by $L = 10(3m-1)$ and $L = 10(3m+1)$, $m = 1,2,3,4,\dots$; (II) there are CF magic numbers that do not correspond to downward cusps in the EXD calculations (marked by medium-size downward arrows in the figures). This happens because cusps associated with L's whose difference from L_0 is divisible by 6 (but not simultaneously by 5) progressively weaken and completely disappear in the intervals $\mathcal{I}_m$ with $m \geq 3$; only cusps with the difference $L - L_0$ divisible by 5 survive. On the other hand, the CF model predicts the appearance of four magic numbers with $L - L_0$ divisible solely by 6 in every interval $\mathcal{I}_m$, at $L = 30m \mp 9$ and $30m \mp 3$, $m = 1,2,3,\dots$. The overall extent of the inadequacy of the CF model can be appreciated better by the fact that there are six false predictions (long and medium-size downward arrows) in every interval $\mathcal{I}_m$ with $m \geq 3$, compared to only five correct ones (small downward arrows; see Fig. 3 and Fig. 4).

In contrast to the CF model, the magic angular momenta in the REM theory are associated with the polygonal ring configurations of N classical point charges. This is due to the fact that the enhanced stability of the downward cusps results from the coherent collective rotation of the regular-polygon REM structures. Due to symmetry requirements, such collective rotation can take place only at magic-angular-momenta values. The in-between angular momenta require the excitation of additional degrees of freedom (like the center of mass and/or vibrational modes), which raises the total energy with respect to the values associated with the magic angular momenta.

For $N = 6$, the lowest in energy ring configuration is the (1,5), while there exists a (0,6) isomer[41,42] with higher en-

ergy. As a result, our EXD calculations (as well as earlier ones[9,11,13] for lower angular momenta $L \lesssim 70$) have found that there exist two sequences of magic angular momenta: a *primary* one (S_p) with $L = 15 + 5m$ [see Eq. (5)], associated with the most stable (1,5) classical molecular configuration, and a *secondary* one (S_s) with $L = 15 + 6m$ [see Eq. (3)], associated with the metastable (0,6) ring arrangement. Furthermore, our calculations (see also Refs. 11 and 13) show that the secondary sequence S_s contributes only in a narrow range of the lowest angular momenta; in the region of higher angular momenta, the primary sequence S_p is the only one that survives and the magic numbers exhibit a period of five units of angular momentum. It is interesting to note that the initial competition between the primary and secondary sequences, and the subsequent prevalence of the primary one, has been seen in other sizes as well:[11] i.e., $N = 5, 7, 8$. Furthermore, this competition is reflected in the field-induced molecular phase transitions associated with broken-symmetry UHF solutions in a parabolic QD. Indeed, Ref. 17 demonstrated recently that, as a function of increasing B, the UHF solutions for $N = 6$ first depict the transformation of the maximum-density droplet[68] into the (0,6) molecular configuration; then (at higher B) the (1,5) configuration replaces the (0,6) structure as the one having the lower HF energy.[69]

The extensive comparisons in this subsection lead inevitably to the conclusion that the CF model cannot explain the systematic trends exhibited by the magic angular momenta in 2D QD's in high magnetic fields. These trends, however, were shown to be a natural consequence of the formation of REM's and their metastable isomers.

B. Radial electron densities

We turn now our attention to a comparison of the radial electron densities (ED's). Figure 5 displays the corresponding ED's from EXD, REM, and CF-JL wave functions at three representative total angular momenta: i.e., $L = 75$ ($\nu = 1/5$), 105 (1/7), and 135 (1/9).

An inspection of Fig. 5 immediately reveals that (I) the EXD radial ED's (solid lines) exhibit a prominent oscillation corresponding to the (1,5) molecular structure (averaged over the azimuthal angles) (indeed the integral of the exact ED's from the origin to the minimum point between the two humps is practically equal to unity); (II) there is very good agreement between the REM (dashed lines) and exact ED's; this agreement improves with higher angular momentum; and (III) the JL ED's (dotted lines) miss the oscillation of the exact ED in all three cases in a substantial way.

The inability of the radial ED's calculated with the JL functions to capture the oscillations exhibited by the exact ones was also seen recently for the $\nu = 1/3$ case and for all electron numbers $N = 6, 7, 8, 9, 10, 11, 12$ in Ref. 62 (see in particular Fig. 1 therein). We further note that the oscillations of the exact ED's in that figure correspond fully to the classical molecular ring arrangements listed in Ref. 41—e.g., to (1,7) for $N = 8$ and to (3,9) for $N = 12$—in agreement with our rotating-electron-molecule interpretation.
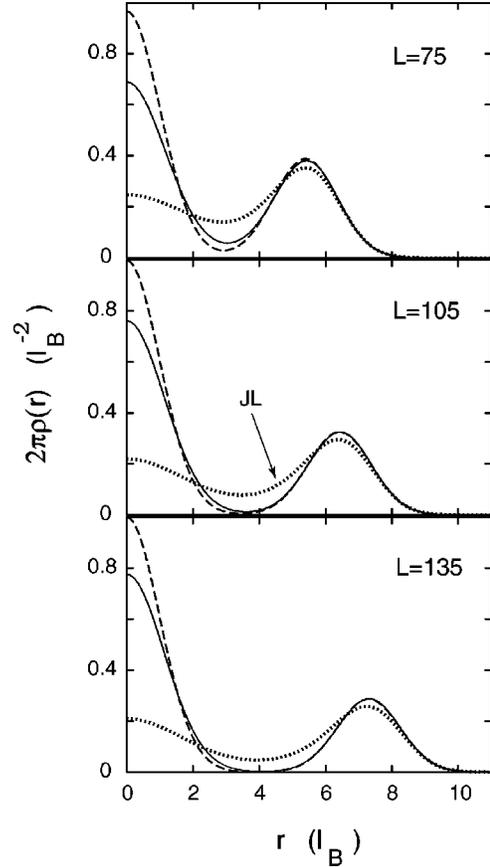
FIG. 5. Radial electron densities for $N = 6$ electrons in high magnetic field. Solid line: densities from exact diagonalization. Dashed line: densities from REM wave functions. Dotted line: densities from Jastrow-Laughlin wave functions.

C. Distribution of occupation numbers

In this subsection, we address the behavior of the occupation-number distribution $n(l) = \langle \Phi | a_l^\dagger a_l | \Phi \rangle$ as a function of the single-particle angular momentum l, where the creation and annihilation operators refer to the single-electron states $\psi_{0,l}(z)$ in the LLL. For $N = 6$, Fig. 6 displays the $n(l)$'s from all three families of wave functions—i.e., EXD (solid circles), REM (open circles), and JL (crosses)—and for the three representative angular momenta $L = 75$ ($\nu = 1/5$), 105 (1/7), and 135 (1/9).

Again, an inspection of Fig. 6 immediately reveals that (I) the EXD occupation numbers exhibit a prominent oscillation corresponding to the (1,5) molecular structure (indeed the sum of the exact $n(l)$'s from $l = 0$ to the minimum point between the two humps is practically equal to unity); (II) there is very good agreement between the REM and exact occupation numbers; this agreement improves with higher angular momentum; and (III) for all three cases, the JL occupation numbers exhibit a systematically different trend and they are not able to capture the oscillatory behavior of the EXD occupation numbers.

We further note that a substantial discrepancy between JL and EXD occupation numbers was also noted in Ref. 64 for the case of $N = 7$ electrons and $\nu = 1/3$ ($L = 63$).
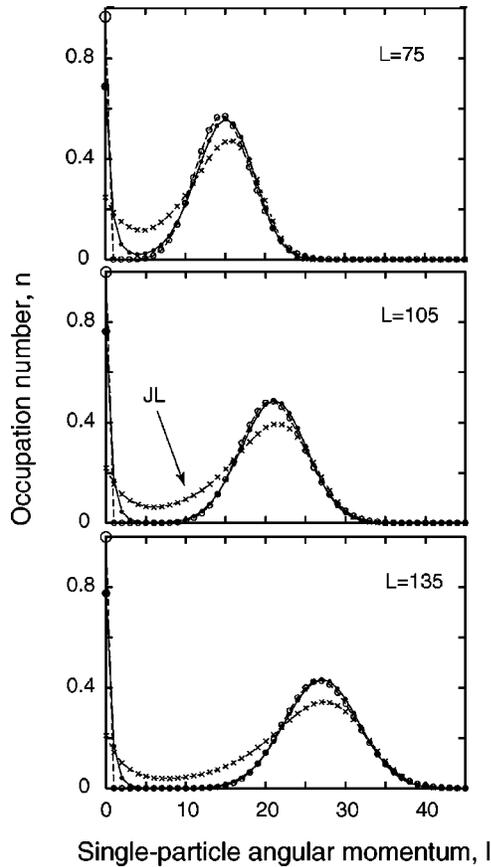
FIG. 6. Distribution of occupation numbers as a function of single-particle angular momentum l for $N=6$ electrons in high magnetic field. Solid circles: occupation numbers from exact diagonalization. Open circles: occupation numbers from REM wave functions. Crosses: occupation numbers from Jastrow-Laughlin wave functions.

The systematic deviations between the JL and EXD ED's and occupation numbers inevitably point to the conclusion that these two families of wave functions represent very different many-body physical problems. Indeed, the JL functions have been found[22] to be exact solutions for a special class of *short-range* two-body forces, while the EXD functions faithfully reflect the *long-range* character of the Coulombic interelectron repulsion. On the other hand, as discussed in Ref. 15, the REM wave functions, derived through a traditional many-body approach, are able to capture the correlations arising from the long-range character of the Coulomb force; the oscillatory behavior of the EXD and REM ED's and occupation numbers (associated with formation of Wigner molecules) constitutes a prominent and unmistaken signature of such Coulombic correlations.

D. Comparison of overlaps and total energies

We turn now our attention to the overlaps of the REM and JL wave functions with those obtained through exact diagonalization. We start by listing in Table II the overlaps for the simpler case of $N=3$ electrons in high magnetic fields. One sees immediately that these overlaps are all very close to

TABLE II. Case of $N=3$ electrons in high magnetic fields. Overlaps, $\langle\Phi_L|\Phi_L^{EX}\rangle/(\langle\Phi_L|\Phi_L\rangle\langle\Phi_L^{EX}|\Phi_L^{EX}\rangle)^{1/2}$, of REM's ($\Phi$'s) and JL functions ($\Phi$'s) with the corresponding exact eigenstates (Φ^{EX}'s) for various values of the angular momenta L (ν are the corresponding fractional filling factors). Recall that the angular momenta for the JL functions are $L^{JL}=N(N-1)(2m+1)/2$, with $m=0,1,2,3,\ldots$. The JL overlaps are from Ref. 1.

$L(\nu)$	JL	REM
9(1/3)	0.999 46	0.983 47
15(1/5)	0.994 68	0.994 73
21(1/7)	0.994 76	0.996 74
27(1/9)	0.995 73	0.997 58
33(1/11)	0.996 52	0.998 07
39(1/13)	0.997 08	0.998 39

unity ($\geqslant 0.99$) for both the REM and JL cases and for even rather high angular momenta [e.g., $L=39$ ($\nu=1/13$)].

Ever since they were calculated by Laughlin in his original paper,[1] the JL overlaps for $N=3$ electrons have exercised a great influence in the literature of the fractional quantum Hall effect. Indeed, in a rather sweeping generalization to any N and L (note that Ref. 62 has indeed found that the JL overlaps for $\nu=1/3$ remain very close to unity for all cases with $5\leqslant N\leqslant 12$), the close-to-unity values of the JL overlaps have been presumed to provide ''proof'' that the CF-JL functions approximate very well the corresponding exact many-body wave functions; as we have already shown earlier, this presumption is highly questionable.

We have calculated the overlaps for $N=6$ electrons and for the three representative higher-angular-momentum values $L=75$ ($\nu=1/5$), 105 (1/7), and 135 (1/9); the results are listed in Table III for both the REM and JL wave functions. A most remarkable feature of the results in Table III is that the extraordinary, higher than 0.99 values (familiar from Laughlin's paper[1]) are totally absent. Instead, the JL overlaps rapidly deteriorate for higher L's (lower ν's), and for $\nu=1/9$ they have attained values below 0.67. In contrast, the REM overlaps remain above 0.80 and slowly approach unity as L increases.

From our results for $\nu\leqslant 1/5$ and the results of Ref. 62 for $\nu=1/3$, it is apparent that the overlaps alone are not a reliable index for assessing the agreement or disagreement between trial and exact wave functions. For example, for $N=6$ and $L=75$ ($\nu=1/5$), Table III shows that the JL and REM overlaps are close to each other (0.837 vs 0.817). However, as earlier analyses based on the electron densities and

TABLE III. Overlaps of JL and REM wave functions with the exact ones for $N=6$ electrons and various angular momenta L (ν are the corresponding fractional filling factors).

$L(\nu)$	JL	REM
75(1/5)	0.837	0.817
105(1/7)	0.710	0.850
135(1/9)	0.665	0.860

TABLE IV. Total interaction energies of JL, REM, and exact diagonalization wave functions for $N=6$ electrons and various angular momenta L (ν are the corresponding fractional filling factors). The percentages within parentheses indicate relative errors. Recall that the angular momenta for the JL functions are $L^{JL}=N(N-1)(2m+1)/2$, $m=0,1,2,3,\ldots$. Energies in units of $e^2/\kappa l_B$, where κ is the dielectric constant.

$L(\nu)$	JL	REM	Exact
75(1/5)	2.2093 (0.32%)	2.2207 (0.85%)	2.2018
85(3/17)		2.0785 (0.65%)	2.0651
95(3/19)		1.9614 (0.55%)	1.9506
105(1/7)	1.8618 (0.46%)	1.8622 (0.48%)	1.8533
115(3/23)		1.7767 (0.45%)	1.7692
125(3/25)		1.7020 (0.38%)	1.6956
135(1/9)	1.6387 (0.50%)	1.6361 (0.34%)	1.6305

occupation numbers show, the JL wave function is not a good approximation to the exact one; in contrast, the REM wave function offers a much better description.

In addition to the overlaps, earlier studies (see, e.g., Ref. 44) have also relied on the total energies for assessing the agreement, or not, between CF and exact wave functions. We thus list in Table IV the total energies for $N=6$ and for the three representative higher-angular-momentum values $L=75$ ($\nu=1/5$), 105 (1/7), and 135 (1/9). It is seen that both the JL and REM total energies exhibit very small relative errors compared to the corresponding EXD ones in all three instances, a fact that indicates that, by themselves, the total energies[70] are an even less reliable index compared to the overlaps. In particular, note that for $N=6$ and $L=135$, the JL and exact total energies differ only in the third decimal point, while at the same time the JL overlap is only 0.665 (see Table III).

E. Exponents of the current-voltage power law

Another quantity of theoretical and experimental interest is the ratio

$$\alpha = \frac{n(l_{max}^{JL}-1)}{n(l_{max}^{JL})} \tag{14}$$

of the corresponding occupation numbers at $l_{max}^{JL}-1$ and l_{max}^{JL}. The interest in this ratio is due to the following two facts: (I) the value of α for the JL function at different fractional fillings has a particular analytic value;[71-73] i.e., it is given by $\alpha^{JL}(\nu)=1/\nu=2m+1$, $m=1,2,3,4,\ldots$; and (II) α happens to enter as the exponent[72,73] of the voltage in the current-voltage law $I \propto V^{\alpha}$ for external electron tunneling into an edge of a fractional quantum Hall system. Recent investigations have found that both the experimental[74] and computed[73] EXD value of α at $\nu=1/3$ deviates from the JL prediction of 3, being in all instances somewhat smaller (i.e., ~ 2.7).

Table V displays the values of α for $N=6$ and for the JL, REM, and EXD wave functions at various values of the total angular momentum L. We have checked that our numerical

TABLE V. Values of the ratio α [Eq. (14)] for JL, REM, and exact diagonalization wave functions for $N=6$ electrons and various angular momenta L; ν (given in parentheses) are the corresponding fractional filling factors. Recall that the angular momenta for the JL functions are $L^{JL}=N(N-1)(2m+1)/2$, $m=0,1,2,3,\ldots$.

$L(\nu)$	JL	REM	Exact
75(1/5)	5.000	1.964	2.877
105(1/7)	7.000	1.972	2.708
135(1/9)	9.000	1.978	2.726

values for α^{JL} (derived by dividing the proper n^{JL}'s; see Fig. 6) are equal to $2m+1$ within numerical accuracy. As seen from Table V, a most striking weakness of the JL functions is that the corresponding α^{JL}'s diverge as $L \to \infty$, a behavior which contrasts sharply with the EXD values that remain at all times finite and somewhat smaller than 3. Such a dramatic difference in behavior should be possible to be checked experimentally. Furthermore, we note that the REM values, although somewhat smaller, are close to the EXD ones and remain bounded as $L \to \infty$.

We conclude that this dramatic qualitative and quantitative weakness of the JL functions is due to their being exact solutions of a family of short-range interparticle forces.[22] On the other hand, as we have stressed earlier in this paper and in Ref. 15, the REM functions are able to capture the essential effects of the correlations associated with the long-range Coulomb force; thus, in agreement with the EXD results, the REM α values remain finite as $L \to \infty$.

V. SUMMARY

Exact diagonalization results for the lowest rotational band of a circular QD with $N=6$ electrons in strong magnetic fields were reported[75] in the range of high angular momenta, $70 \leq L \leq 140$ (covering the corresponding range of fractional filling factors, $1/5 \geq \nu \geq 1/9$). These EXD results were used in a thorough assessment of the ability of the composite-fermion[4]–Jastrow-Laughlin[1] and rotating-electron-molecule[15] trial wave functions to approximate the exact wave functions in the case of 2D QD's.

A detailed comparison (addressing five properties: i.e., prediction of magic angular momenta, radial electron densities, occupation number distributions, overlaps and total energies, and exponents of current-voltage power law) shows that the REM many-body wave functions provide a description that is superior to that obtained through the CF-JL ones. An important finding is that "global" quantities (like overlaps and total energies) are not particularly reliable indices for comparing exact and trial wave functions; a reliable decision on the agreement, or lack of it, between exact and trial wave functions should include detailed comparisons of quantities like radial electron densities and/or occupation number distributions.

We finally note that the CF-JL wave functions have been most useful for the modeling of the bulk fractional quantum Hall effect. However, theoretical investigations concerning

the bulk system have unavoidably, due to computational limitations, relied on finite-size systems to assess the *validity* of the CF-JL wave functions. Thus it is natural to conjecture that the unexpected finding of this paper—i.e., that the CF-JL functions exhibit remarkable weaknesses in reproducing the exact wave functions of QD's in high B—may have ramifications for our present understanding of the fractional quantum Hall effect itself. Investigations of such probable ramifications and related questions concerning the domain of validity of the REM and CF-JL wave functions in the bulk will be addressed in future publications. In the present paper, we focused on the case of QD's, which constitute a theoretically self-contained problem when exact diagonalization calculations become available; in the near future, a wider range of such calculations will be within reach, due to new generations of powerful computers.

---

*Electronic address: Constantine.Yannouleas@physics.gatech.edu

†Electronic address: Uzi.Landman@physics.gatech.edu

[1] R.B. Laughlin, Phys. Rev. Lett. **50**, 1395 (1983).

[2] R.B. Laughlin, Phys. Rev. B **27**, 3383 (1983).

[3] S.M. Girvin and T. Jach, Phys. Rev. B **28**, 4506 (1983).

[4] J.K. Jain, Phys. Rev. B **41**, 7653 (1990).

[5] S.-R. Eric Yang, A.H. MacDonald, and M.D. Johnson, Phys. Rev. Lett. **71**, 3194 (1993).

[6] J.K. Jain and T. Kawamura, Europhys. Lett. **29**, 321 (1995).

[7] T. Kawamura and J.K. Jain, J. Phys.: Condens. Matter **8**, 2095 (1996).

[8] H.-M. Müller and S.E. Koonin, Phys. Rev. B **54**, 14 532 (1996).

[9] T. Seki, Y. Kuramoto, and T. Nishino, J. Phys. Soc. Jpn. **65**, 3945 (1996).

[10] P.A. Maksym, Phys. Rev. B **53**, 10 871 (1996).

[11] W.Y. Ruan and H-F. Cheung, J. Phys.: Condens. Matter **11**, 435 (1999).

[12] C. Yannouleas and U. Landman, Phys. Rev. B **61**, 15 895 (2000).

[13] P.A. Maksym, H. Imamura, G.P. Mallon, and H. Aoki, J. Phys.: Condens. Matter **12**, R299 (2000).

[14] C.E. Creffield, J.H. Jefferson, S. Sarkar, and D.L.J. Tipton, Phys. Rev. B **62**, 7249 (2000).

[15] C. Yannouleas and U. Landman, Phys. Rev. B **66**, 115315 (2002).

[16] M. Rontani, G. Goldoni, F. Manghi, and E. Molinari, Europhys. Lett. **58**, 555 (2002).

[17] B. Szafran, S. Bednarek, and J. Adamowski, Phys. Rev. B **67**, 045311 (2003).

[18] See, e.g., A. L. Jacak, P. Hawrylak, and A. Wojs, *Quantum Dots* (Springer, Berlin, 1998), in particular Chap. 4.5.

[19] R.C. Ashoori, Nature (London) **379**, 413 (1996).

[20] S. Tarucha, D.G. Austing, T. Honda, R.J. van der Hage, and L.P. Kouwenhoven, Phys. Rev. Lett. **77**, 3613 (1996).

[21] L. P. Kouwenhoven, C. M. Marcus, P. L. McEuen, S. Tarucha, R. M. Westervelt, and N. S. Wingreen, in *Mesoscopic Electron Transport*, Vol. 345 of *NATO Advanced Study Institute, Series E*, edited by L. L. Sohn, L. P. Kouwenhoven, and G. Schön (Kluwer, Dordrecht, 1997), p. 105.

[22] F.D.M. Haldane, Phys. Rev. Lett. **51**, 605 (1983); S.A. Trugman and S. Kivelson, Phys. Rev. B **31**, 5280 (1985).

[23] We use the well-known formula $\nu = N(N-1)/2L$ (see Ref. 2), which specifies the corresponding fractional filling factors in the thermodynamic limit. We stress, however, that in this paper we focus exclusively on finite-size systems; thus, throughout this paper, ν is used as a more compact index in place of L.

[24] C. Yannouleas and U. Landman, Phys. Rev. Lett. **82**, 5325 (1999); **85**, 2220(E) (2000).

[25] C.E. Creffield, W. Häusler, J.H. Jefferson, and S. Sarkar, Phys. Rev. B **59**, 10 719 (1999).

[26] R. Egger, W. Häusler, C.H. Mak, and H. Grabert, Phys. Rev. Lett. **82**, 3320 (1999); **83**, 462(E) (1999).

[27] C. Yannouleas and U. Landman, Phys. Rev. Lett. **85**, 1726 (2000).

[28] W. Häusler, B. Reusch, R. Egger, and H. Grabert, Physica B **284**, 1772 (2000).

[29] A.V. Filinov, Y.E. Lozovik, and M. Bonitz, Phys. Status Solidi B **221**, 231 (2000).

[30] S.M. Reimann, M. Koskinen, and M. Manninen, Phys. Rev. B **62**, 8108 (2000).

[31] B. Reusch, W. Häusler, and H. Grabert, Phys. Rev. B **63**, 113313 (2001).

[32] A. Matulis and F.M. Peeters, Solid State Commun. **117**, 655 (2001).

[33] A.V. Filinov, M. Bonitz, and Y.E. Lozovik, Phys. Rev. Lett. **86**, 3851 (2001).

[34] C. Yannouleas and U. Landman, J. Phys.: Condens. Matter **14**, L591 (2002).

[35] P.A. Sundqvist, S.Y. Volkov, Y.E. Lozovik, and M. Willander, Phys. Rev. B **66**, 075335 (2002).

[36] S.A. Mikhailov and K. Ziegler, Eur. Phys. J. B **28**, 117 (2002).

[37] S.A. Mikhailov, Physica E (Amsterdam) **12**, 884 (2002).

[38] S.A. Mikhailov, Phys. Rev. B **65**, 115312 (2002).

[39] A. Harju, S. Siljamaki, and R.M. Nieminen, Phys. Rev. B **65**, 075309 (2002).

[40] C. Yannouleas and U. Landman, Phys. Rev. B **68**, 035325 (2003).

[41] V.M. Bedanov and F.M. Peeters, Phys. Rev. B **49**, 2667 (1994).

[42] F. Bolton and U. Rössler, Superlattices Microstruct. **13**, 139 (1993).

[43] Under conditions of partial spin polarization (i.e., low magnetic fields), the molecular configurations may exhibit distortions away from the classical equilibrium configurations. With increasing R_W, however, the classical molecular configurations are recovered (see Ref. 38).

[44] J.K. Jain and R.K. Kamilla, Int. J. Mod. Phys. B **11**, 2621 (1997).

[45] E. Goldmann and S.R. Renn, Phys. Rev. B **56**, 13 296 (1997).

[46] S.-R. Eric Yang and J.H. Han, Phys. Rev. B **57**, R12 681 (1998).

[47] M. Taut, J. Phys.: Condens. Matter **12**, 3689 (2000).

[48] M. Manninen, S. Viefers, M. Koskinen, and S.M. Reimann, Phys. Rev. B **64**, 245322 (2001).

[49] X. Wan, K. Yang, and E.H. Rezayi, Phys. Rev. Lett. **88**, 056802 (2002).

[50] X. Wan, E.H. Rezayi, and K. Yang, cond-mat/0302341 (unpublished).

[51] A. Harju, S. Siljamaki, and R.M. Nieminen, Phys. Rev. Lett. **88**, 226804 (2002).

[52] P. Ring and P. Schuck, *The Nuclear Many-body Problem* (Springer, New York, 1980) Chap. 11, and references therein.

[53] C. Yannouleas and U. Landman, Eur. Phys. J. D **16**, 373 (2001).

[54] C. Yannouleas and U. Landman, Int. J. Quantum Chem. **90**, 699 (2002).

[55] K. Maki and X. Zotos, Phys. Rev. B **28**, 4349 (1983).

[56] The definition $z \equiv x + \iota y$ is associated with positive angular momenta for the single-particle states in the lowest Landau level. In Ref. 15, we used $z \equiv x - \iota y$ and negative single-particle angular momenta in the lowest Landau level. The final expressions for the trial wave functions do not depend on these choices.

[57] Both the finite-size REM molecule and several sophisticated bulk Wigner crystal (BWC) approaches at high B (listed at the end of this footnote) start with a single-determinantal UHF wave function constructed out of the orbitals in Eq. (1), and both do improve it by introducing additional correlations; however, the nature of these correlations is quite different between the REM and BWC approaches. Indeed, due the the finite size of the system, the REM approach includes correlations associated with fluctuations in the *azimuthal* angle (see Ref. 15 and 40); these correlations arise from the restoration of the circular symmetry and result in states with good total angular momenta (in particular *magic* angular momenta; see Sec. IV A). Naturally, in the BWC approaches, angular momentum conservation and magic angular momenta are not considered; for example, Lam and Girvin include correlations from *vibrational*-type fluctuations of the BWC that are more in tune with the expected translational invariance of a bulk system. As a result, the REM exhibits drastically different properties from the properties of an N-electron piece of the bulk Wigner crystal. Rather, the REM wave functions exhibit properties associated with the incompressible magic angular momentum states in the spectra of QD's, which are finite-size *precursors* to the "correlated-liquid" fractional quantum Hall states of the bulk (see Ref. 18). For sophisticated BWC approaches at high B, see, e.g., P.K. Lam and S.M. Girvin, Phys. Rev. B **30**, 473 (1984); H. Yi and H.A. Fertig, *ibid.* **58**, 4019 (1998).

[58] C.G. Darwin, Proc. Cambridge Philos. Soc. **27**, 86 (1930); V. Fock, Z. Phys. **47**, 446 (1928).

[59] In the case of $N = 6$ electrons, we have used 338, 5444, 32 134, and 118 765 terms in this decomposition for $L = 45$ ($\nu = 1/3$), 75 (1/5), 105 (1/7), and 135 (1/9), respectively. These numbers correspond to all the Slater determinants with $L = 15(2m + 1)$ and individual angular momenta $l \leq l_{max}^{JL} = 5(2m + 1)$, including the cases with zero coefficients. We remind the reader that $l_{max}^{JL} = (2m + 1)(N - 1)$ is the maximum individual angular momentum allowed in the JL states. The Slater decomposition of the JL states for $N = 2, 3, 4, 5, 6$, but only for $\nu = 1/3$, has been reported earlier in G.V. Dunne, Int. J. Mod. Phys. B **7**, 4783 (1993).

[60] S. Wolfram, *Mathematica: A System for Doing Mathematics by Computer* (Addison-Wesley, Reading, MA, 1991).

[61] M. Stone, H.W. Wyld, and R.L. Schult, Phys. Rev. B **45**, 14 156 (1992).

[62] E.V. Tsiper and V.J. Goldman, Phys. Rev. B **64**, 165311 (2001).

[63] M. Kasner, Ann. Phys. (Berlin) **11**, 175 (2002), and references therein.

[64] V.A. Kashurnikov, N.V. Prokof'ev, B.V. Svistunov, and I.S. Tupitsyn, Phys. Rev. B **54**, 8644 (1996).

[65] E.V. Tsiper, J. Math. Phys. **43**, 1664 (2002).

[66] R. B. Lehoucq, D. C. Sorensen, and C. Yang, *ARPACK Users' Guide: Solution of Large-Scale Eigenvalue Problems with Implicitly Restarted Arnoldi Methods* (SIAM, Philadelphia, 1998).

[67] Reference 9 gives the full list of the nine CF magic numbers in the interval ($1 \geq \nu \geq 1/3$). Reference 6 excludes two of them: i.e., the CF magic angular momenta 27 and 33.

[68] A.H. MacDonald, S.R.E. Yang, and M.D. Johnson, Aust. J. Phys. **46**, 345 (1993).

[69] At $B = 0$, the interelectron Coulombic repulsion can also induce (as a function of increasing R_W) a similar succession of phase transitions [i.e., normal fluid $\rightarrow$ (0,6) molecule $\rightarrow$ (1,5) molecule]; see Fig. 2 in Ref. 24.

[70] There is no "variational dilemma" from the fact that the CF-JL and REM functions are two essentially different wave functions with very close expectation values of the energy. Indeed, the CF-JL wave functions correspond to a Hamiltonian with short-range two-body interactions, while the REM functions correspond to the actual Hamiltonian of the Coulomb problem that involves long-range interelectron interactions. Therefore these represent two separate variational problems.

[71] S. Mitra and A.H. MacDonald, Phys. Rev. B **48**, 2005 (1993).

[72] X.G. Wen, Phys. Rev. B **41**, 12 838 (1990); Int. J. Mod. Phys. B **6**, 1711 (1992).

[73] V.J. Goldman and E.V. Tsiper, Phys. Rev. Lett. **86**, 5841 (2001).

[74] A.M. Chang, M.K. Wu, C.C. Chi, L.N. Pfeiffer, and K.W. West, Phys. Rev. Lett. **86**, 143 (2001), and references therein.

[75] We have specifically considered the limit when the confining potential can be neglected compared to the confinement induced by the high magnetic field. In high B, the effect of the confining potential amounts simply in selecting a specific magic angular momentum state (see Sec. IV A) as the ground state of the system (the specific value of the magic L depends on the strength of B and the parameters of the confinement). In most studies (see, e.g., Ref. 6, Ref. 9, or Ref. 13), the external confinement has been modeled as a harmonic potential. Most recently, however, Wan *et al.* (Ref. 49 and Ref. 50) have studied few-electron QD's taking into consideration a disklike neutralizing positive background. Indeed, these authors employ a confining potential arising from a positive background charge distributed uniformly on a parallel disk at a distance d from the electron layer (the typical d in experiments is $d \geq 10 l_B$; see Ref. 50). As was the case with the harmonic external potential, these authors found again that their external confinement influences which magic-L state becomes the ground state of the system. Most importantly, the ground-state wave functions in their exact diagonalization study exhibit strong oscillations in the radial electron density (in an apparent agreement with the classical ring configurations of Wigner molecules) and in disagreement with the CF-JL wave functions. It is interesting to note the coincidence, for all practical purposes, of the exact radial electron density for $N = 6$ and

$L=105$ calulated by Wan *et al.* with that calculated by us [compare Fig. 5(d) in Ref. 50 with the middle panel of Fig. 5 in this paper]. In order to account for the disagreement between the exact and CF-JL wave functions, Wan *et al.* were led to use the concept of "edge reconstruction." In the case studied by us, however, our exact diagonalization results (and those of Tsiper and Goldman; see Ref. 62) do not include any external confinement, a fact that rules out "edge reconstruction" as the under-

lying cause for the disagreement between the exact and CF-JL wave functions. As we have pointed out in this paper previously (see Sec. IV E and also Ref. 15), this disagreement arises from the fact that the CF-JL functions do not capture the long-range character of the Coulomb interelectron repulsion. On the contrary the REM wave functions are able to capture the long-range Coulombic correlations and thus are in better agreement with the wave functions from exact diagonalization.